TRENDS IN SCIENCES 2025; 22(9): 10238
https://doi.org/10.48048/tis.2025.10238
RESEARCH ARTICLE

pH-Engineered Tm^{3+}/Yb^{3+} Co-Doped TiO_2: Morphological and Structural Properties Transformation and Photocatalytic Degradation Activity Performance

Nurina Izzati Md Rapi[1], Amira Syahida Zulkifli[1], Nur Syazwani Mohd Zailani[1], Muhammad Syahmi Basir[1], Mohd Zaki Mohd Yusoff[1,2,3] and Suraya Ahmad Kamil[1,2,*]

[1]Faculty of Applied Sciences, Universiti Teknologi MARA, Selangor 40450, Malaysia
[2]NANO-SciTech Lab, Centre for Functional Materials and Nanotechnology, Institute of Science, Universiti Teknologi MARA, Selangor 40450, Malaysia
[3]Institute for Biodiversity and Sustainable Development, Universiti Teknologi MARA, Selangor 40450, Malaysia

([*]Corresponding author's e-mail: suraya_ak@uitm.edu.my)

Received: 23 March 2025, Revised: 9 April 2025, Accepted: 16 April 2025, Published: 1 July 2025

Abstract

Thulium (Tm^{3+}) and ytterbium (Yb^{3+}) co-doping in TiO_2 has garnered considerable interest among RE dopants because of their distinctive optical characteristics. In this present study, Tm^{3+}/Yb^{3+} co-doped TiO_2 powder was prepared using the sol-gel method by varying pH values (4, 6, 8, and 10). The morphological and structural properties of Tm^{3+}/Yb^{3+} co-doped TiO_2 were analyzed. The photocatalytic performance of the Tm^{3+}/Yb^{3+} co-doped TiO_2 was evaluated in methylene blue (MB) degradation under UV light irradiation. The mixed phase of anatase-brookite was discovered in an acidic medium, while pure anatase was observed at higher pH values. As pH increases, the average crystallite size decreases, and this can be related to the hydrolysis-condensation reactions. FESEM images showed that all samples demonstrate the formation of spherical granules. According to the FTIR analysis, the rising pH value induces a change in Ti-O stretching vibrations towards a lower wavenumber, attributable to the transition of phase from a mixed anatase-brookite to a pure anatase phase. Sample pH 4 exhibited the highest rate constant and photocatalytic degradation percentage because it is a mixed anatase-brookite phase. This enhancement primarily arises from the synergistic effect between the 2 phases. Optimizing the pH during synthesis is critical for tailoring the morphological and structural properties of Tm^{3+}/Yb^{3+} co-doped TiO_2, ultimately improving their photocatalytic efficiency and practical applicability in environmental and energy-related fields.

Keywords: Rare earth, Photocatalytic degradation, Anatase-brookite, Sol-gel, TiO_2

Introduction

Following the groundbreaking discovery by Fujishima and Honda in 1972 of the photoelectrochemical water-splitting reaction utilising semiconductors, the field of photocatalysis has rapidly advanced as a prominent method within advanced oxidation processes (AOPs). This technology is recognised for its energy efficiency, sustainability, and positive impact on the environment. This approach has the potential to address wastewater treatment, which is characterised by significant complexity, low biodegradability, and high pollutant concentrations [1]. Photocatalysis offers numerous benefits compared to traditional water treatment methods, such as the capacity to fully degrade and mineralise dyes and chemicals into CO_2 and H_2O, along with facilitating the degradation of highly stable compounds that pose challenges for other degradation processes. They are capable of operating efficiently under standard room temperature and pressure conditions without the need for a specialised supply of particular gases. One additional advantage of

photocatalysis is its cost-effectiveness compared to other water treatment methods, along with the absence of waste management concerns [2].

Titanium oxide (TiO_2) has been the most frequently utilised photocatalyst among the numerous photocatalysts and has been used extensively in heterogeneous photocatalysis due to its chemical stability, nontoxicity, and affordability. However, TiO_2's wide bandgap (3.0 - 3.2 eV) is one of the drawbacks as a photocatalyst. Because of that, TiO_2 has a limited absorption of visible light, and it also exhibits fast electron (e^-)-hole (h^+) recombination rates. Hence, it is essential to alter the catalyst material by making it less likely for (e^-)/(h^+) pairs to recombine, lowering its band gap, and enhancing optical absorption within the visible spectrum [3]. In pursuit of this objective, a variety of effective approaches were investigated [4-6]. The integration of various elements into TiO_2 is a current approach aimed at mitigating the short lifetimes of photoinduced electron-hole pairs.

Doping TiO_2 with rare earth (RE) metals can substantially alter the physical, chemical and electrical properties of the TiO_2 photocatalyst, thereby impacting its photocatalytic activity [7]. The production of RE metal ion complexes with various Lewis bases such as alcohols, amines, thiols and aldehydes involve the f-orbital electrons, which serve as an efficient substrate for the adsorption of organic pollutants and enhance photocatalytic activity [8]. 4f and 5d electronic configurations of RE metal ions modify the catalytic and optical properties of TiO_2 as reported by Zhang *et al.* [9] and Ranjit *et al.* [10]. This modification occurs through the generation of labile oxygen vacancies with relatively high charge mobility and via redox coupling of $RE^{n+}/RE^{(n-1)+}$, in contrast to the bulk oxygen species within the TiO_2 lattice. The ionic radii of RE metals exceed that of the Ti^{4+} ion, leading to their deposition on the surface of TiO_2. This contributes to the enhancement of the effective surface area of TiO_2. The introduction of RE metal ions has also been documented to diminish the agglomeration of TiO_2 particles. This boosts the availability of active surfaces and elevates the photocatalytic activity. The integration of RE metal ions into the TiO_2 lattice also serves to trap electrons and decreases the rate of e^--h^+ recombination in TiO_2 [8]. Among RE dopants, thulium (Tm^{3+}) and ytterbium (Yb^{3+}) co-doping in TiO_2 has attracted significant attention due to their unique optical properties. Yb^{3+} ions act as efficient sensitizers [11], absorbing near-infrared (NIR) light and transferring energy to Tm^{3+} ions, which can subsequently emit photons in the visible or UV range via upconversion processes [12]. This upconversion mechanism enables TiO_2 to utilize a broader spectrum of sunlight, thereby enhancing its photocatalytic efficiency under visible and NIR light irradiation. Additionally, the introduction of Tm^{3+} and Yb^{3+} can modify the electronic structure of TiO_2, reduce charge carrier recombination, and improve surface defect states, further promoting photocatalytic reactions.

Rutile, anatase, and brookite are the 3 crystallographic phases in which TiO_2 nanoparticles are all found in nature. Anatase (tetragonal TiO_2) demonstrates superior photocatalytic performance compared to rutile (tetragonal) and brookite (orthorhombic). Anatase coexists with a minor proportion of the other 2 phases, rutile and brookite, demonstrating greater photocatalytic efficacy compared to its pure form. It is due to the mixed-phase effect, which promoted the charge separation and hindered the electron-hole recombination [13]. The combination of brookite and anatase phases continues to be intriguing; however, there is a scarcity of reports regarding the photocatalytic activity of mixed-phase anatase-brookite.

On the other hand, the pH of the environment significantly affects titanium dioxide (TiO_2) and their degradation processes. It influences the surface charge, surface chemistry, bandgap energy, and hydroxyl radical generation of TiO_2. Low pH results in positive surface charge, while high pH leads to negative surface charge. According to Tsega and Dejene, under high acidic conditions, brookite, anatase and rutile of TiO_2 coexisted, with rutile as a dominant phase, whereas under low acidic pH, only the anatase phase of TiO_2 was present [14]. Sridevi *et al.* reported the formation of a mixed phase of anatase and brookite, with the anatase phase dominant at pH 6, 8, and 10 [15]. Devi, Kumar and Reddy varied the pH of TiO_2 (pH: 3, 7 and 10) and they revealed that at pH 3, pure rutile was formed, while at pH 7, the anatase and rutile phases coexisted [16]. At pH 10, the anatase phase was favoured. Alam *et al.* [17] observed that only the anatase phase of TiO_2 nanoparticles was formed at pH 2, 2.5, 3.5 and 8.5. However, a mixture of brookite, rutile and anatase was detected to coexist at pH 9.5. Because there are various

phases obtained based on the pH value, this indicates that the effect of pH is complex. Working with rare-earth dopants makes it more critical. Tm^{3+} and Yb^{3+} are both rare earth elements, and their solubility in solution is pH-dependent [18-20]. A well-controlled pH ensures homogeneous doping and reduces defect-induced recombination losses [21]. To the best of our knowledge, there is no study about the effect of pH on morphology, structural and photocatalytic properties of Tm^{3+}/Yb^{3+}co-doped TiO_2 photocatalyst. Therefore, this study is to investigate the effect of pH on the morphological, structural, and photocatalytic properties of Tm^{3+}/Yb^{3+} co-doped TiO_2 photocatalysts. The present study used the sol-gel method to prepare Tm^{3+}/Yb^{3+}co-doped TiO_2 using initial solutions of various pH values (pH = 4, 6, 8, 10).

Materials and methods

Sample preparation

The sol-gel technique was employed to synthesize Tm^{3+}/Yb^{3+} co-doped TiO_2 powder. The sol-gel method is frequently favoured for synthesising TiO_2nanoparticles due to its simplicity, cost-effectiveness, accurate doping control, low-temperature processing and high levels of uniformity and purity in the final product [22,23]. First, 55 mL of ethanol (EtOH) and 26 mL of titanium (IV) butoxide ($Ti(OBu)_4$) were mixed into the 250 mL borosilicate bottle and were left to stir for 1 h. Next, 5 mL of distilled water (DI) and 55 mL of EtOH were combined to a previous solution in the borosilicate container. The mixture was stirred continuously at room temperature for the following 4 h. A total of 10 wt.% of $YbCl_3$ and $TmCl_3$ in a ratio of 9:1 was introduced to the precursor solution. HCl or NaOH were added to make the solution become acidic (pH: 4, 6) and alkaline (pH: 8, 10), respectively. Later, the solution was left to stir overnight to dissolve the powder completely. Then, the solution was peptized for 48 h before having 2 layers of supernatant and Tm^{3+}/Yb^{3+} co-doped TiO_2 precipitate. After that, the precipitation was dried for 2 h at 120 °C to remove the remaining ethanol in the solution. Upon completion of the drying process, the powder was ground into a fine powder for 3 h via a ball mill pulverizer instrument. The powder was then annealed for 3 h at 400 °C at a rate of 5 °C/min. The samples were labelled as YT-T4, YT-T6, YT-T8, and YT-T10 based on their pH values of 4, 6, 8, and 10, respectively.

The pH values (4, 6, 8, 10) were chosen to systematically study their influence on the sol-gel synthesis of Tm^{3+}/Yb^{3+} co-doped TiO_2 photocatalysts. These values cover acidic to alkaline conditions, enabling the analysis of their impact on hydrolysis and condensation rates, phase formation, dopant solubility, and photocatalytic performance. By optimizing the synthesis pH, the aim is to achieve homogeneous doping, minimize recombination losses, and enhance the photocatalytic efficiency of the Tm^{3+}/Yb^{3+}co-doped TiO_2 photocatalysts.

Sample characterization

Thermalgravimetric Analysis (TGA) (Perkin Elmer Pyris 1, USA) with a heating rate of 10 °C/min under ambient air was employed to determine the optimal annealing temperature for Tm^{3+}/Yb^{3+} co-doped TiO_2. The sample was heated from room temperature to 900 °C. The X-ray diffraction (XRD) analysis was performed utilizing PANalytical X'pert PRO (Netherland) with CuKα (λ = 1.54 Å) radiation at 45 kV and an accelerating voltage current of 40 mA. The 2θ scanning range extended from 10° to 90° with a step increment of 0.01°. The Debye-Scherrer equation (Eq. (1)) was used to determine the size of the crystallite [24]:

$$D = \frac{0.94\lambda}{\beta \cos\theta} \quad (1)$$

where D is particle diameter, λ is the wavelength, β is the full width half maximum (FWHM) and θ is the diffraction angle.

The infrared absorption spectrum derived from FTIR (Perkin Elmer FTIR Spectrum One, USA) was used to identify the chemical bonds in the samples. Elemental composition and surface morphologies of the samples were obtained using energy dispersive X-ray (EDX) (Bruker XFlash 6I100 EDX, USA) and field emission scanning electron microscopy (FESEM) (Thermoscientific Apreo 2S FESEM, USA), respectively. Reflectance spectra were recorded by Shimadzu UV-vis diffuse reflectance spectroscopy (Japan) (DRS) at a wavelength range of 200 - 2500 nm. The energy band gap was estimated using the Kubelka-

Munk function, F(R) (Eq. (2)) and Tauc and Davis-Mott relation (Eq. (3)) [25].

$$F(R) = \frac{(1-R)^2}{2R} \quad (2)$$

$$(F(R)hv)^n = A(hv - E_g) \quad (3)$$

where F(R) is a coefficient of absorption, R is a reflectance in %, E_g is an energy band gap, hv is a photon energy, B is constant and n is a factor that depends on electron transition characteristic.

Photocatalytic degradation testing

The activity of photocatalytic degradation was examined utilizing a UV light (Analytikjena, UVP UVGL-58, 6 W, 365 nm) as the light source and methylene blue (MB) serving as a dye. The separation between the UV lamp and the MB solution is 5 cm. 70 mL of a 10 ppm MB solution (10 mg/L) at pH 8.75 was introduced into the petri dish. Then, 200 mg of the Tm^{3+}/Yb^{3+} co-doped TiO_2 was dispersed into the MB solution and the mixture was constantly stirred for 30 min in the dark condition to reach adsorption-desorption equilibrium during the photocatalyst-dye reaction. After that, the dye with photocatalyst was exposed to the UV light and the photocatalytic degradation activity was carried out for 120 min with approximately 2 mL of MB solution withdrawn at each 10 min interval. The aliquots were then scanned using a Thermo Scientific Genesys 30 single beam visible spectrophotometer. The percentage of photocatalytic degradation was determined using Eq. (4) [26]:

$$Percentage\ of\ photodegradation\ (\%) of\ MB = \frac{C_o - C}{C_o} \times 100\ \% \quad (4)$$

where C_o is the MB solution concentration while C is the MB solution concentration after reaction time.

Results and discussion

Figure 1 displays the TGA patterns of Yb^{3+}/Tm^{3+} doped TiO_2 before the annealing process. The TGA curve in **Figure 1** depicts the weight loss (%) as a function of temperature rise. According to the TGA plot, there are 3 distinct phases to the total weight loss (%). The evaporation of water molecules causes the initial stage of weight loss, which occurs between ambient temperature and 160 °C. Weight loss at this temperature range is around 8.88 %. The second stage of weight loss around 4.63 % occurs between 160 and 400 °C is associated to the decomposition of organic compounds [27]. There is barely any weight loss at temperatures greater than 400 °C (third stage). The amorphous phase will change to crystalline further heating above 400 °C [28,29]. The samples are calcined at above 400 °C, which is considered an appropriate annealing temperature given TGA studies as it is stable at this temperature range. The TGA pattern curve and weight loss are similar to those observed in the previous study on co-doped TiO_2 synthesised via the sol-gel technique [30-32].

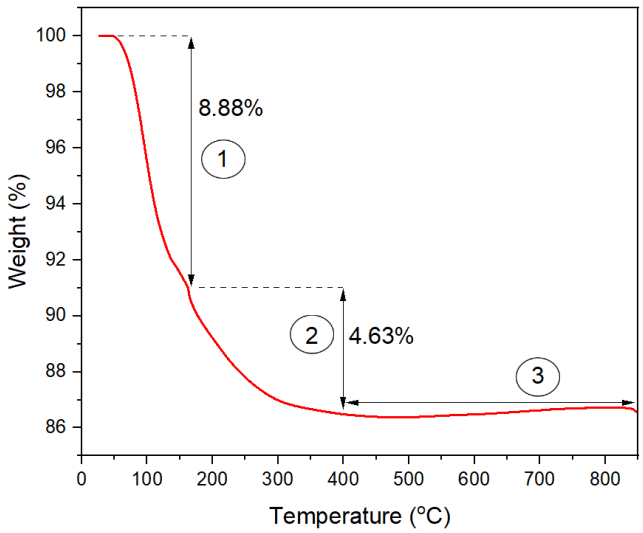

Figure 1 TGA curve of Tm^{3+}/Yb^{3+} doped TiO_2 before annealing process.

The XRD pattern shown in **Figure 2** confirms that the produced photocatalyst contains TiO_2 polymorphs such as anatase and brookite. The diffraction peaks of pure anatase phase are observed at 2θ values of 25.3°, 37.8°, 48.0°, 54.0°, 54.9°, 62.6°, 68.5°, 70.1°, 75.0° and 82.6° correspond to the crystal plane of (101), (004), (200), (105), (211), (204), (116), (220), (215), and (224), respectively as indexed in the JCPDS file no. 01-071-1166 for samples YT-T6, YT-T8 and YT-T10. Meanwhile, the additional diffraction peaks of the brookite phase which are (211) and (302) (JCPDS file no. 01-076-1937) are identified for the pH 4 sample. As pH values increased, the brookite diffraction peaks disappeared. At pH 6, 8, and 10, the TiO_2 powders exhibited solely the anatase phase. The mixed anatase-brookite phase is more likely to develop under moderate acidic conditions [5,14]. It is because, under moderate acidic environment, H^+ ions tend to slow down the hydrolysis of titanium precursors. This can stabilize the intermediate species that facilitate the production of the brookite phase [33]. This is similar to the findings by Szołdra *et al.* [34] and Tsega and Degene [14],who discovered brookite tends to form in acidic environments. On the other hand, similar findings were stated by Yalcin [35] and Cassaignon *et al.* [36], where mixed phases were achieved when TiO_2 was prepared in an acidic environment, while a pure anatase phase was favored in a higher pH environment

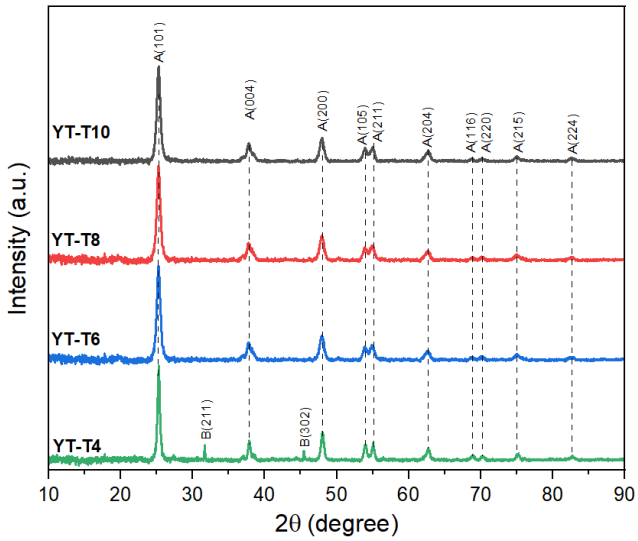

Figure 2 XRD diffraction pattern of Tm^{3+}/Yb^{3+} co-doped TiO_2 NPs at different pH.

As pH increases, the average crystallite size decreases, as seen in **Table 1** and **Figure 3**. This can be elucidated through hydrolysis-condensation activities. In very acidic conditions, bigger crystallites tend to develop due to the highly condensation reactions exhibited by the low hydrolyzed species [37]. Nevertheless, increased alkalinity promotes nucleation, resulting in the creation of colloidal solutions and, consequently, a reduced crystallite size. The findings align closely with those documented by several researchers [37,38].

Table 1 Average crystallite size, FWHM and specific surface area for different pH of Tm^{3+}/Yb^{3+} co-doped TiO_2.

Sample (pH)	FWHM (2θ)	Average crystallite size (±0.01 nm)	Specific surface area (m^2/g)
4 (YT-T4)	0.41	39.00	36.37
6 (YT-T6)	0.57	28.09	50.50
8 (YT-T8)	0.61	26.25	54.04
10 (YT-T10)	0.62	25.83	54.91

The specific surface area (SSA) was calculated using the total area covered by the crystals in unit mass in Eq. (5) [24]:

$$SSA = \frac{6 \times 10^3}{\rho D_\rho} \quad (5)$$

where ρ is the density of materials and D_ρ is the size of the crystallite.

The estimated specific surface area value is exhibited in **Table 2**, and the relationship between the crystallite size and SSA is shown in **Figure 3**. Alkaline conditions promote the development of smaller crystallites size, resulting in a larger surface area that can enhance the availability of active sites for photocatalytic reactions. An increased surface area enhances the material's capacity to engage with light, a critical factor in photocatalysis. A greater exposed surface area allows for the absorption of more photons, leading to the generation of additional electron-hole pairs, which in turn propels the photocatalytic reaction.

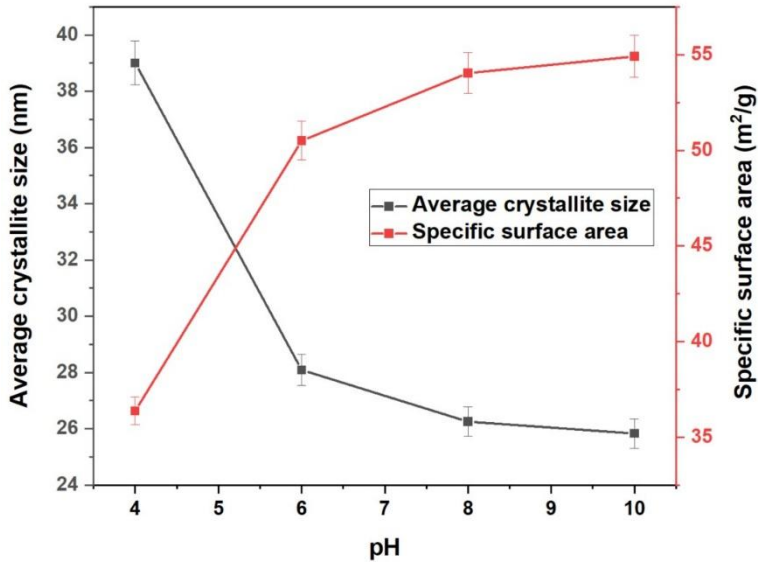

Figure 3 The relationship of pH with the specific surface area and crystallite size.

Figure 4 depicts the surface morphology of Tm^{3+}/Yb^{3+} co-doped TiO_2 obtained from FESEM. All samples demonstrate the formation of spherical granules. According to the FESEM image and **Table 2**, particle size decreases as the pH increases. The phenomenon occurs due to the agglomeration of the NPs, which can be attributed to the Van der Waals attraction or repulsion forces of electrostatics. It is suggested that the attractive forces prevailed at lower pH, whereas at pH 10, the repulsive forces outweighed the attractive forces, leading to a reduction in particle agglomeration [39,40].

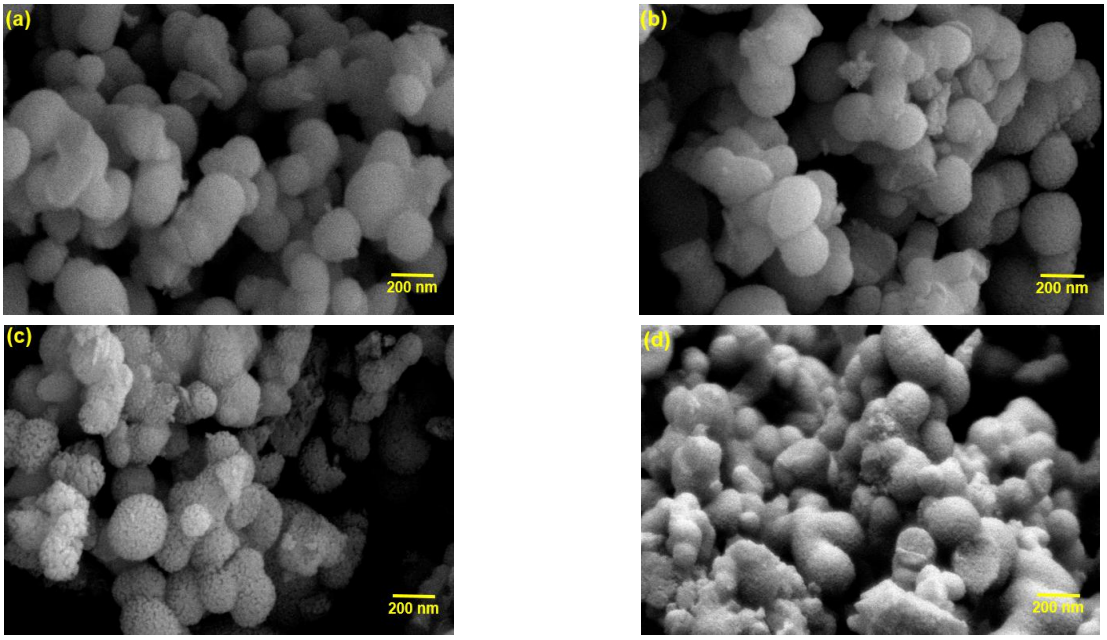

Figure 4 Surface morphology by FESEM of Tm^{3+}/Yb^{3+} co-doped TiO_2 synthesized at different pH (a) pH 4, (b) pH 6, (c) pH 8, (d) pH 10.

Table 2 Average particle size of Tm^{3+}/Yb^{3+} co-doped TiO_2 synthesized at different pH.

Sample (pH)	Average particle size (nm)
4 (YT-T4)	275.71 ± 58.03
6 (YT-T6)	258.38 ± 38.98
8 (YT-T8)	200.04 ± 73.73
10 (YT-T10)	170.79 ± 50.35

Table 3 shows the elemental composition of Tm^{3+}/Yb^{3+} co-doped TiO_2 for all samples obtained from EDX analysis. All elements present in the samples were detected. The ratio Yb:Tm is almost similar to 9:1. All samples showed similar element concentrations, and it can be concluded that the difference in pH does not significantly affect the element content in the samples. The FTIR spectra of Tm^{3+}/Yb^{3+} co-doped TiO_2 was displayed in **Figure 5**. The transmittance peaks at approximately 3400 and 1630 cm^{-1} correspond to O-H stretching and bending, respectively [41]. Ti-O and Ti-O-Ti stretching vibrations were identified in the infrared region ranging from 500 to 800 cm^{-1} [42]. According to the dashed line in **Figure 5**, the rising pH value induces a change in Ti-O stretching vibrations towards a lower wavenumber, attributable to the transition of phase from a mixed anatase-brookite to a pure anatase phase. Anatase and brookite exhibit distinct Ti–O bond lengths and crystal structures, which influence their vibrational modes. Brookite exhibits a more distorted octahedral structure, resulting in higher wavenumber vibrations when compared to anatase. Upon the removal of brookite, the structure transitions to pure anatase, characterized by a more symmetric TiO_6 octahedral unit, leading to a vibrational mode with lower energy (lower wavenumber) [33]. Meanwhile, the absorption band at 1358 cm^{-1} is ascribed to the stretching mode of CH_3 bonds [43].

Table 3 Elemental composition of Tm^{3+}/Yb^{3+} co-doped TiO_2 (pH 4).

Sample (pH)	Ti (wt.%)	O (wt.%)	Tm (wt.%)	Yb (wt.%)
4 (YT-T4)	47.06	48.08	0.50	4.36
6 (YT-T6)	45.87	49.01	0.54	4.58
8 (YT-T8)	46.56	48.46	0.48	4.50
10 (YT-T10)	47.13	47.86	0.49	4.52

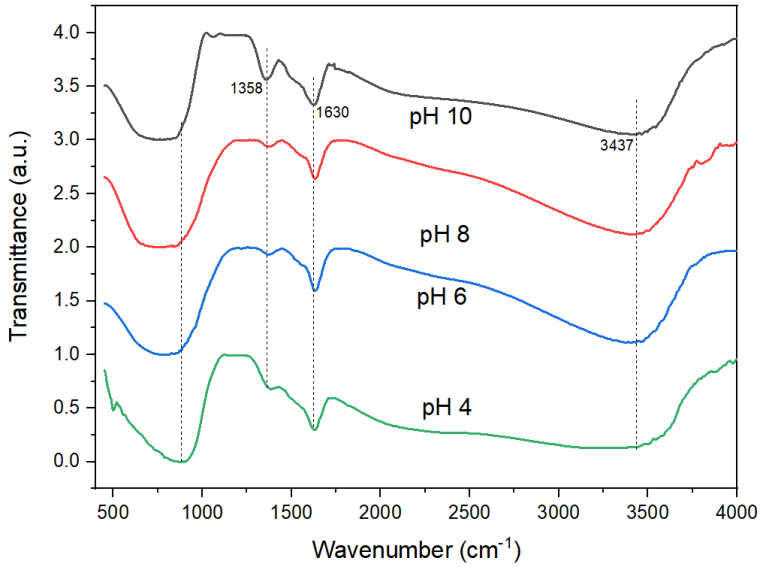

Figure 5 FTIR spectra of Tm^{3+}/Yb^{3+} co-doped TiO_2 with varying pH value.

The photocatalytic performance of the Tm^{3+}/Yb^{3+} co-doped TiO_2 was evaluated in methylene blue (MB) degradation under UV light irradiation. The changes in absorbance value are observed at the absorbance peak at wavelength 664 nm of aqueous MB. **Figures 6(a) - 6(d)** illustrates the variations in the absorption spectra of MB dye over time for each sample. The peak at 664 nm diminishes progressively with the duration of UV light exposure, leading to sample pH 4 demonstrating the greatest photocatalytic efficiency. This outcome aligns with the photocatalytic degradation percentage and rate constant in the degradation of 10 ppm MB, as shown in **Figures 7(a)** and **7(b)**. Sample pH 4 demonstrates the highest degradation percentage, achieving 99.98 % of MB with a rate constant of 7.45×10^{-3} min^{-1} as tabulated in **Table 4**. The rate constant was calculated using Eq. (6) [26]:

$$\ln\left(\frac{C_0 - C_t}{C_0}\right) = kt \quad (6)$$

where C_0 represents the initial concentration of MB, while C_t denotes the MB concentration after the photocatalytic reaction has occurred at a specific time (t) and k is the rate constant.

The solution of degradation of MB before and after is shown in **Figure 8**. It shows that after 2 h; all the MB solution becomes clear. Sample pH 4 shows the highest degradation and rate constant because it is a mixed anatase-brookite phase. The mixed phase of anatase and brookite typically demonstrates enhanced photocatalytic activity for the degradation of methylene blue in comparison to pure anatase. This improvement primarily arises from the synergistic effect between the 2 phases, as shown in **Figure 9**. The formation of a bi-phase junction structure within the mixed phase leads to a difference in the band gap, subsequently enhancing the separation efficiency of photoelectrons and holes,

thereby improving photocatalytic performance [13,35,36]. Additionally, brookite possesses the suitable electron trapping depth that could facilitate the activation of the majority of electrons when exposed to light illumination [13]. The study reported by Ioannidou *et al.* [44], Zhou *et al.* [45] and Lu *et al.* [46] also mentioned mixed phase of anatase-brookite have higher photocatalytic efficiency compared to pure anatase.

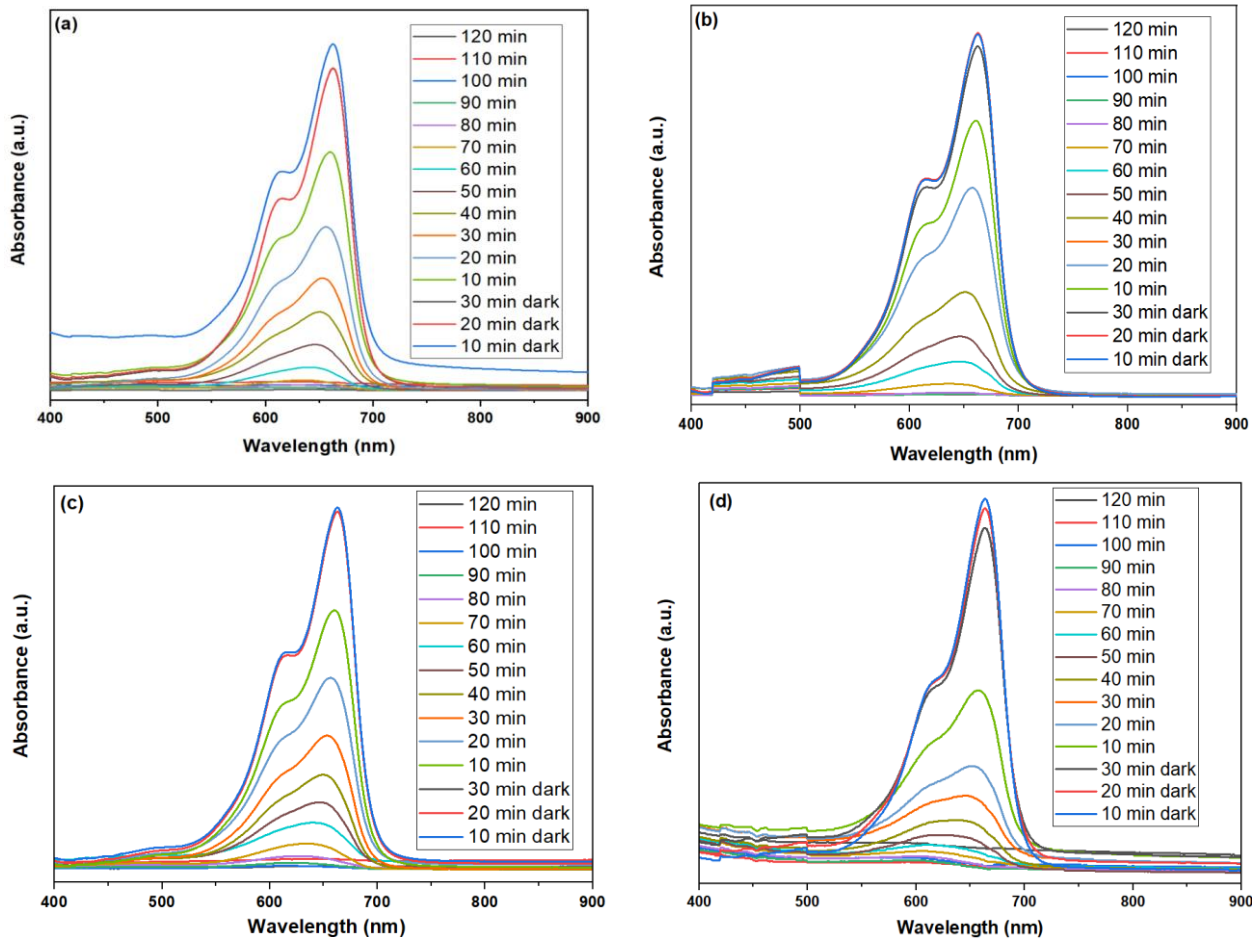

Figure 6 The absorbance vs wavelength for degradation of MB of sample (a) pH 4, (b) pH 6, (c) pH 8, and (d) pH 10.

Table 4 Photocatalytic degradation percentage and rate constant for Tm^{3+}/Yb^{3+} co-doped TiO_2 photocatalysts under UV Irradiation.

Sample (pH)	Photocatalytic Degradation (%)	Photocatalytic Rate Constant (min^{-1})
4 (YT-T4)	99.98	$(7.45 \pm 0.03)\times10^{-3}$
6 (YT-T6)	99.83	$(6.12 \pm 0.02)\times10^{-3}$
8 (YT-T8)	99.36	$(4.94 \pm 0.02)\times10^{-3}$
10 (YT-T10)	98.12	$(3.98 \pm 0.01)\times10^{-3}$

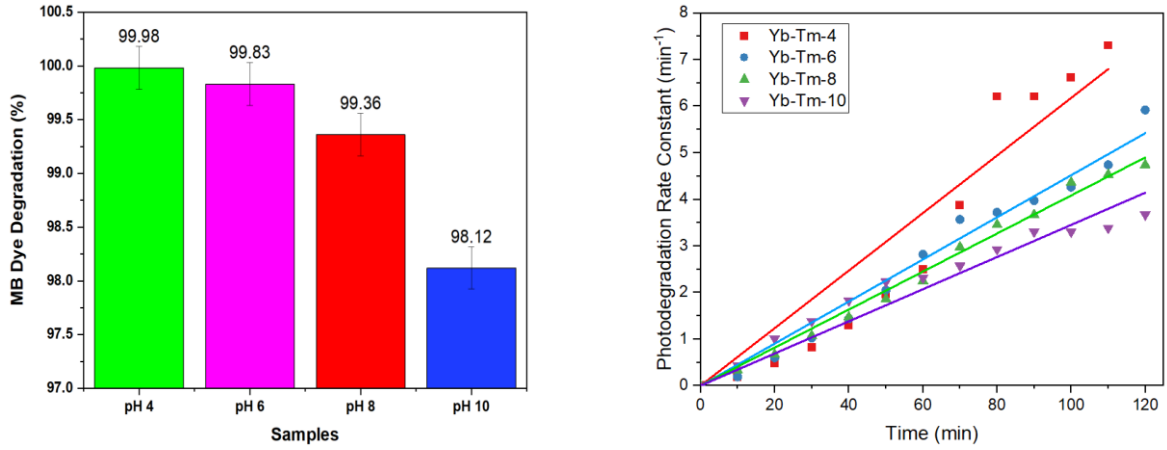

(a) (b)

Figure 7 Photocatalytic degradation analysis of all samples (pH 4 - 10) in 10 ppm MB under UV light: (a) photodegradation percentage and (b) rate constant.

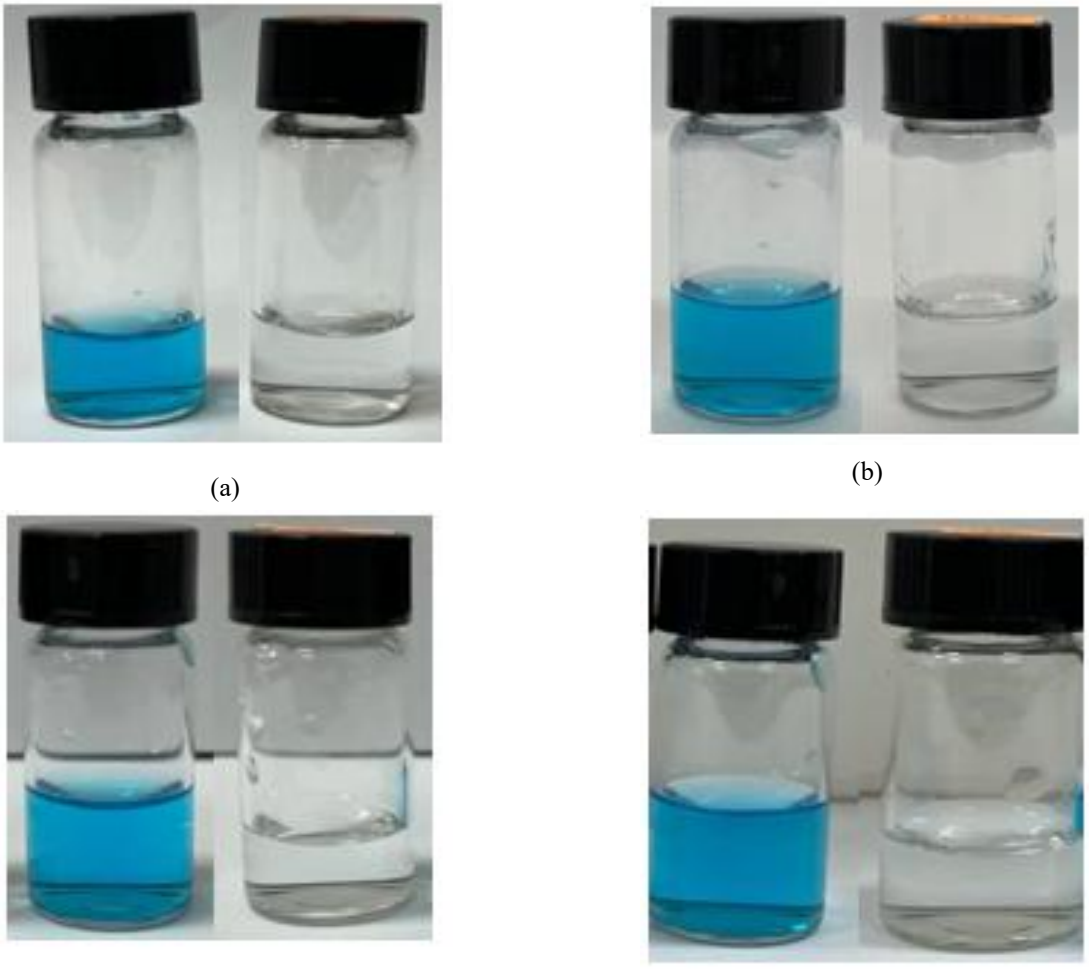

(a) (b)

(c) (d)

Figure 8 The evolution of photodegradation of MB under UV light irradiation for samples synthesized with different pH: (a) pH 4, (b) pH 6, (c) pH 8, and (d) pH 10.z

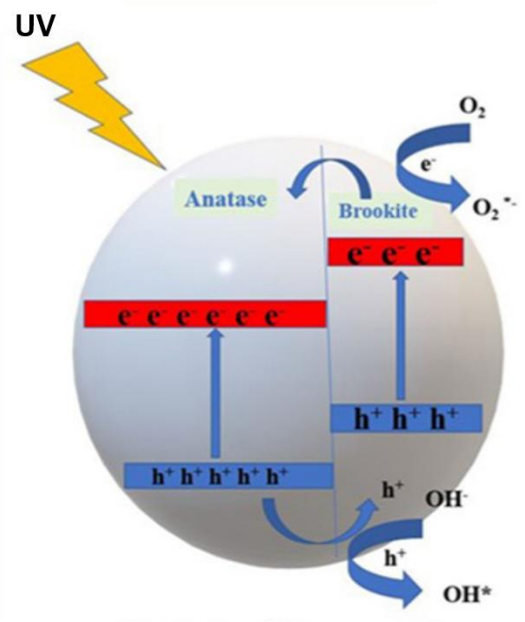

Figure 9 Proposed mechanism illustrating electron transfer in mixed-phase anatase-brookite [47].

Conclusions

At pH 4, both anatase and brookite phases were present, whereas the pure anatase phase was detected to form at pH 6, 8 and 10. With an increase in pH, there is a corresponding decrease in the average crystallite size, which can be attributed to the hydrolysis-condensation reactions. The FESEM images reveal that all samples exhibit formation of spherical granules. As illustrated in FTIR analysis, the increasing pH value causes a shift in Ti-O stretching vibrations to a lower wavenumber, due to the phase transition from a mixed anatase-brookite to a pure anatase phase. Sample pH 4 demonstrates the most significant photocatalytic degradation and rate constant due to its composition as a mixed anatase-brookite phase. This improvement mainly results from the synergistic interaction between the 2 phases. Adjusting the pH during synthesis is essential for optimizing the morphological and structural characteristics of Tm^{3+}/Yb^{3+} co-doped TiO_2, which in turn enhances their photocatalytic efficiency and practical use in environmental and energy applications.

Acknowledgements

The authors would like to thank the Faculty of Applied Sciences, Universiti Teknologi MARA, Malaysia for assistance and facilities throughout the research. This research was not funded by any grant.

References

[1] WS Koe, JW Lee, WC Chong, YL Pang and LC Sim. An overview of photocatalytic degradation: photocatalysts, mechanisms, and development of photocatalytic membrane. *Environmental Science and Pollution Research* 2020; **27**, 2522-2565.

[2] MA Al-Nuaim, AA Alwasiti and ZY Shnain. The photocatalytic process in the treatment of polluted water. *Chemical Papers* 2023; **77**, 677-701.

[3] D Komaraiah, E Radha, J Sivakumar, MVR Reddy and R Sayanna. Photoluminescence and photocatalytic activity of spin coated Ag^+ doped anatase TiO_2 thin films. *Optical Materials* 2020; **108**, 110401.

[4] D Gogoi, A Namdeo, AK Golder and NR Peela. Ag-doped TiO_2 photocatalysts with effective charge transfer for highly efficient hydrogen production through water splitting. *International Journal of Hydrogen Energy* 2020; **45(4)**, 2729-2744.

[5] LKT Navarro and C Jaroslav. Enhancing photocatalytic properties of TiO_2 photocatalyst and heterojunctions: a comprehensive review of the impact of biphasic systems in aerogels and xerogels synthesis, methods, and mechanisms for environmental applications. *Gels* 2023; **9(12)**, 976.

[6] L Li, X Chen, X Quan, F Qiu and X Zhang. Synthesis of CuO_x/TiO_2 photocatalysts with enhanced photocatalytic performance. *ACS Omega* 2023; **8(2)**, 2723-2732.

[7] J Prakash, Samriti, A Kumar, H Dai, BC Janegitz, V Krishnan, HC Swart and S Sun. Novel rare earth metal–doped one-dimensional TiO_2 nanostructures: fundamentals and multifunctional applications. *Materials Today Sustainability* 2021; **13**, 100066.

[8] NU Saqib, R Adnan and I Shah. A mini-review on rare earth metal-doped TiO_2 for photocatalytic remediation of wastewater. *Environmental Science and Pollution Research* 2016; **23**, 15941-15951.

[9] Y Zhang, H Zhang, Y Xu and Y Wang. Significant effect of lanthanide doping on the texture and properties of nanocrystalline mesoporous TiO_2. *Journal of Solid State Chemistry* 2004; **177(10)**, 3490-3498.

[10] KT Ranjit, I Willner, SH Bossmann and AM Braun. Lanthanide oxide doped titanium dioxide photocatalysts: Effective photocatalysts for the enhanced degradation of salicylic acid and t-cinnamic acid. *Journal of Catalysis* 2001; **204(2)**, 305-313.

[11] PCJ Clark, E Andresen, MJ Sear, M Favaro, L Girardi, RVD Krol, U Resch-Genger and DE Starr. Quantification of the activator and sensitizer ion distributions in $NaYF_4$:Yb^{3+}, Er^{3+} upconverting nanoparticles via depth-profiling with Tender X-ray Photoemission. *Small* 2022; **18(29)**, 2107976.

[12] RF Falci, TC Ranquine, NO Dantas, V Anjos and MJV Bell. Upconversion and near infrared emission in Yb–Tm mediated by ZnTe crystals in oxide glasses. *Optical Materials* 2022; **124**, 111843.

[13] Z Liu, H Ouyang, J Hu, W Chen, J Cheng, J Pang, S Liu and R Tan. Engineering anatase/brookite TiO_2 heterophase junctions via nitrogen doping to improve photocatalytic transfer hydrogenation. *Industrial and Engineering Chemistry Research* 2024; **63(31)**, 13491-13502.

[14] M Tsega and FB Dejene. Influence of acidic pH on the formulation of TiO_2 nanocrystalline powders with enhanced photoluminescence property. *Heliyon* 2017; **3(2)**, e00246.

[15] DV Sridevi, KT Ramya Devi, N Jayakumar and E Sundaravadivel. pH dependent synthesis of TiO_2 nanoparticles exerts its effect on bacterial growth inhibition and osteoblasts proliferation. *AIP Advances* 2020; **10**, 095119.

[16] GS Devi, KA Kumar and KS Reddy. Effect of pH on synthesis of single-phase titania (TiO_2) nanoparticles and its characterization. *Particulate Science and Technology* 2015; **33(3)**, 219-223.

[17] MA Alam, RK Bishwas, S Mostofa, and SA Jahan. Crystallographic phase stability of nanocrystalline polymorphs TiO_2 by tailoring hydrolysis pH. *South African Journal of Chemical Engineering* 2024; **49**, 73-85.

[18] J Kastenhofer, O Spadiut, VG Papangelakis and DG Allen. Roles of pH and phosphate in rare earth element biosorption with living acidophilic microalgae. *Applied Microbiology and Biotechnology* 2024; **108(1)**, 262.

[19] G Senanayake, S Jayasekera, AMTS Bandara, E Koenigsberger, L Koenigsberger and J Kyle. Rare earth metal ion solubility in sulphate-phosphate solutions of pH range −0.5 to 5.0 relevant to processing fluorapatite rich concentrates: Effect of calcium, aluminium, iron and sodium ions and temperature up to 80 °C. *Minerals Engineering* 2016; **98**, 169-176.

[20] S Cunningham, M Etherington-Rivas and G Azimi. Solubility of neodymium and dysprosium sulfates at different pH and temperature and the effect of yttrium sulfate, sodium sulfate, and ammonium sulfate mixtures: Strengthening the predictive capacities of the OLI software. *Hydrometallurgy* 2024; **224**, 106253.

[21] S Zhang, X Yi, G Hu, M Chen, H Shen, B Li, L Yang, W Dai, J Zou and S Luo. Configuration regulation of active sites by accurate doping inducing self-adapting defect for enhanced photocatalytic applications: A review. *Coordination Chemistry Reviews* 2023; **478**, 214970.

[22] S Mugundan, P Praveen, S Sridhar, S Prabu, KL Mary, M Ubaidullah, SF Shaikh and S Kanagesan. Sol-gel synthesized barium doped TiO, nanoparticles for solar photocatalytic application.

Inorganic Chemistry Communications 2022; **139**, 109340.

[23] D Bokov, AT Jalil, S Chupradit, W Suksatan, MI Ansari, If Shewael,GH Valiev and E Kianfar. Nanomaterial by sol-gel method: synthesis and application. *Advances in Materials Science and Enginecring* 2021; **2021(1)**, 5102014.

[24] MS Basir, SN Supardan and SA Kamil. Effect of annealing temperature on the structural, morphological, photocatalytic and optical properties of the Cu-Ni co-doped TiO_2 nanoparticles. *Digest Journal of Nanomaterials and Biostructures* 2023; **18(3)**, 841-857.

[25] RMA Iqbal, T Akhtar, E Sitara, H Nasir, A Fazal, U Rafique, S Ullah and A Mehmood. Development of $Ag_{0.04}ZrO_2$/rGO heterojunction, as an efficient visible light photocatalyst for degradation of methyl orange. *Scientific Report* 2022; **12**, 12308.

[26] S Rajendran, GK Inwati, E Sitara, VK Yadav, N Choudhary, MB Solanki, MH Albellattif, KK Yadav, N Gupta, S Islam and B Jeon. Enriched catalytic activity of TiO_2 nanoparticles supported by activated carbon for noxious pollutant elimination. *Nanomaterials* 2021; **11(11)**, 2808.

[27] S Balaji, R Guda, BK Mandal, M Kasula, E Ubba and FRN Khan. Green synthesis of nano-titania (TiO_2 NPs) utilizing aqueous Eucalyptus globulus leaf extract: Applications in the synthesis of 4H-pyran derivatives. *Research on Chemical Intermediates* 2021; **47**, 3919-3931

[28] D Rajkumar, H Umamahesvari and P Nagaraju. Micro spherical anatase phase TiO_2 thin films for room temperature operated formaldehyde gas sensor applications. *Results in Chemistry* 2023; **5**, 100946.

[29] F Jonas, B Lebcau, L Michelin, C Carteret, L Josien, L Vidal, S Rigolet, P Gaudin and J Blin. Thermal stability and phase transformation of semi-crystalline mesostructured TiO_2 in the presence of heteroelements. *Microporous and Mesoporous Materials* 2021; **315**, 110896.

[30] B Toubal, R Bensaha and F Yakuphanoglu. The influence of copper-cobalt co-doping on optical and clectrical properties of nanostructures TiO_2 thin films prepared by sol-gel. *Journal of Sol-Gel Science and Technology* 2017; **82(2)**, 478-489.

[31] A Siddiqa, D Masih, D Anjum and M Siddiq. Cobalt and sulfur co-doped nano-size TiO_2 for photodegradation of various dyes and phenol. *Journal of Environmental* Sciences 2015; **37**, 100-109.

[32] X Zhu, L Pei, R Zhu, Y Jiao, R Tang and W Feng. Preparation and characterization of Sn/La co-doped TiO_2 nanomaterials and their phase transformation and photocatalytic activity. *Scientific Reports* 2018; **8**, 12387.

[33] FS Freyria, N Blangetti, S Esposito, R Nasi, M Armandi, V Annelio and B Bonelli. Effects of the brookite phase on the properties of different nanostructured TiO_2 phases photocatalytically active towards the degradation of N-Phenylurea. *ChemistryOpen* 2020; **9(9)**, 903-912.

[34] P Szoldra, M Frac, R Lach, L Zych, M Radecka, A Trenczek-Zajac and W Pichor. Effect of brookite on the photocatalytic properties of mixed-phase TiO: Obtained at a higher temperature. *Materials Science and Enginecring: B* 2023; **287**, 116104.

[35] M Yalcin. The effect of pH on the physical and structural properties of TiO_2 nanoparticles. *Journal of Crystal Growth* 2022; **585**, 126603.

[36] S Cassaignon, M Koelsch and JP Jolivet. From TiCl, to TiO_2 nanoparticles (anatase, brookite and rutile): Thermohydrolysis and oxidation in aqueous medium. *Journal* of *Physics and Chemistry of Solids* 2007; **68(5-6)**, 695-700.

[37] N Khima, A Chelouche, F Challali, D Djouadi, A Djermoune, M Luce, A Cricenti, D Becerril, S Bellucci and T Touam. TiO_2 sol–gel thin films: Effect of acidic and basic pH on physical characteristics. *Journal of Sol-Gel Science and Technology* 2024; **112**, 277-288.

[38] P Dulian, W Nachit, J Jaglarz, P Zieba, J Kanak and W Zukowski. Photocatalytic methylene blue degradation on multilayer transparent TiO_2 coatings. *Optical Materials* 2019; **90**, 264-272.

[39] F Azeez, E Al-Hetlani, M Arafa, Y Abdelmonem, AA Nazeer, MO Amin and M Madkour. The effect of surface charge on photocatalytic degradation of methylene blue dye using chargeable titania nanoparticles. *Scientific Reports* 2018; **8**, 7104.

[40] KAD Guzman, MP Finnegan and JF Banfield. Influence of surface potential on aggregation and transport of titania nanoparticles. *Environmental Science and Technology* 2006; **40(24)**, 7688-7693.

[41] MRA Kumar, B Abebe, HP Nagaswarupa, HCA Murthy, CR Ravikumar and FK Sabir. Enhanced photocatalytic and electrochemical performance of TiO_2-Fe_2O_3 nanocomposite: its applications in dye decolorization and as supercapacitors. *Scientific Reports* 2020; **10**, 1249.

[42] S Arunmetha, NR Dhineshbabu, A Kumar and R Jayavel. Preparation of sulfur doped TiO_2 nanoparticles from rutile sand and their performance testing in hybrid solar cells. *Journal of Materials Science: Materials in Electronics* 2021; **32**, 28382-28393.

[43] P Singla, A Gupta, K Singh and OP Pandey. Influence of anatase-brookite composition on photocatalytic degradation of diethyl phthalate. *Ceramic International* 2021; **47(21)**, 30702-30710.

.

[44] T Ioannidou, M Anagnostopoulou, IA Vasiliadouand, C Marchal, E Alexandridou, V Keller and KC Christoforidis. Mixed phase anatase nanosheets/brookite nanorods TiO_2 photocatalysts for enhanced gas phase CO_2 photoreduction and H_2 production. *Journal of Environmental Chemical Engineering* 2024; **12(1)**, 111644.

[45] H Zhao, L Liu, JM Andino and Y Li. Bicrystalline TiO_2 with controllable anatase-brookite phase content for enhanced CO2 photoreduction to fuels. *Journal of Materials Chemistry A* 2013; **1(28)**, 8209-8216.

[46] X Lu, D Mao, X Wei, H Zhang, J Xie and W Wei. Tunable synthesis of enhanced photodegradation activity of brookite/anatase mixed-phase titanium dioxide. *Journal of Materials Research* 2013; **28(3)**, 400-404.

[47] MS Monisha and R Sreeja. Anatase-Brookite mixed phase TiO_2 nanoparticles for the photocatalytic degradation of methylene blue. *Iranian Journal of Catalysis* 2024; **14(4)**, 142440-142441.